arXiv:cond-mat/0507421v2 [cond-mat.stat-mech] 22 Sep 2005

Structural Studies of Decaying Fluid Turbulence: Effect of Initial Conditions

Chirag Kalelkar*
Centre for Condensed Matter Theory, Department of Physics,
Indian Institute of Science, Bangalore 560012, India.

We present results from a systematic numerical study of structural properties of an unforced, incompressible, homogeneous, and isotropic three-dimensional turbulent fluid with an initial energy spectrum that develops a cascade of kinetic energy to large wavenumbers. The results are compared with those from a recently studied set of power-law initial energy spectra [C. Kalelkar and R. Pandit, Phys. Rev. E, **69**, 046304 (2004)] which do not exhibit such a cascade. Differences are exhibited in plots of vorticity isosurfaces, the temporal evolution of the kinetic energy-dissipation rate, and the rates of production of the mean enstrophy along the principal axes of the strain-rate tensor. A crossover between non-'cascade-type' and 'cascade-type' behaviour is shown numerically for a specific set of initial energy spectra.

PACS numbers: 47.27.Gs

I. INTRODUCTION

Studies of structural properties (in space) of a turbulent fluid may lead to an understanding of dynamically significant processes in turbulence. Homogeneous and isotropic turbulence, within the context of *statistically steady* flows, has been the subject of extensive laboratory[1] and numerical[2, 3, 4] studies. These studies show that the turbulent fluid has a kinetic energy spectrum with a wavenumber range that exhibits a power-law with exponent equal to $-5/3$, in accordance with a phenomenological theory due to Kolmogorov[5, 6]. In the statistical steady state, visualization of the vorticity field reveals that regions of intense vorticity are organized in slender filaments[1, 2, 3, 4]. The vorticity vector is observed to preferentially align[7] with the eigenvector associated with the intermediate eigenvalue of the strain-rate tensor of the fluid. By contrast, systematic spatial studies of *decaying* turbulence are scarce and restricted to numerical studies[8, 9] of vorticity isosurfaces with initial energy spectra of the type that develop a cascade of kinetic energy to large wavenumbers.

A recent study[10], investigated the decay of unforced, incompressible, homogeneous, and isotropic three-dimensional magnetohydrodynamic turbulence from power-law initial conditions. The study was a generalization of results[11] obtained for the corresponding fluid case. In particular, it was shown both analytically and numerically, that for the power-law initial energy spectrum $E(k,t_0) \sim k$ ($k = |\mathbf{k}|$ is the magnitude of the wave vector and $t = t_0$ is the choice of virtual origin of time), the kinetic energy $E(t)$ was found to decay as t^{-1} and the integral length scale $L(t)$ was found to grow as $t^{0.5}$. Such power-law initial conditions are of interest in the astrophysical context of the decay of 'primordial' energy spectra[12]. It was shown numerically[10], that such an initial energy spectrum does not develop a cascade to large wavenumbers; however, structural properties had not been probed.

In this paper, we present results from a pseudospectral direct-numerical simulation (DNS) of the unforced, incompressible, three-dimensional Navier-Stokes equations and contrast spatial results obtained from an initial energy spectrum that develops a cascade (Section II), with results from the power-law initial spectrum (Section III) mentioned above. Plots of vorticity isosurfaces are found to differ, with distinct filaments in regions of intense vorticity, lacking in the case with power-law initial spectrum. The temporal evolution of the kinetic energy-dissipation rate and the rates of production of the mean enstrophy along the principal axes of the strain-rate tensor, are also found to differ. However, preferential alignment of the vorticity vector with the intermediate eigenvector of the strain-rate tensor is found to be unchanged. We also compare some classical results on mean enstrophy production in decaying turbulence. We show numerically that a crossover between the above-mentioned cases may be realised with an appropriate choice of initial conditions.

The Navier-Stokes equations in vorticity form are

$$\frac{D\omega_i}{Dt} = S_{ij}\omega_j + \nu \frac{\partial^2 \omega_i}{\partial x_j \partial x_j}, \tag{1}$$

where $D/Dt \equiv \partial_t + v_j\partial_j$ is the material derivative, ν is the kinematic viscosity, $S_{ij} \equiv 1/2(\partial_j v_i + \partial_i v_j)$ is the strain-rate tensor, and $\omega_i \equiv \epsilon_{ijk}\partial_j v_k$ is the vorticity (ϵ_{ijk} is the Levi-Civita tensor), $i, j, k = 1, 2, 3$, with a summation implicit over repeated indices. We enforce the incompressibility condition $\partial_i v_i = 0$.

II. CASCADE-TYPE SPECTRUM

A. Numerical Method

We use a pseudospectral method[13] to solve Eqs. (1) numerically, in a cubical box of side 2π with periodic boundary conditions and 192^3 Fourier modes. We do not address issues pertaining to the scaling of higher-order structure functions of velocity differences or investigate dissipation-scale properties, and believe that our spectral resolution is adequate for the types of studies that we have carried out. For the temporal evolution, we use an Adams-Bashforth scheme (step size $\delta t = 10^{-3}$) with double-precision arithmetic and set $\nu = 10^{-5}$. We include a hyperviscous term of the form $\nu_h \nabla^4 \mathbf{v}$ in Eqs. (1), with $\nu_h = 10^{-6}$. We show explicitly in Section II(C), that our results are unaffected by inclusion of hyperviscosity. The initial velocity field is taken to be $\mathbf{v}(\mathbf{k}, t_0) \sim k^2 e^{-k^2} e^{i\theta_{\mathbf{k}}}$, with $\theta_{\mathbf{k}}$ random variables distributed uniformly between 0 and 2π. This corresponds to an initial energy spectrum $E(k, t_0) \sim k^4 e^{-2k^2}$ (with $E(k,t) \equiv |\mathbf{v}(\mathbf{k}, t)|^2$, the one-dimensional spectrum), which is a convenient choice that develops a cascade to large wavenumbers (see below). We measure time in units of the initial large-eddy turnover time $\tau_0 \equiv 2\pi / v^0_{rms}$ (here τ_0 equals 4.23), $v^0_{rms} \equiv [\langle \sum_{\mathbf{k}} |\mathbf{v}(\mathbf{k}, t_0)|^2 \rangle]^{1/2}$ is the root-mean-square value of the initial velocity, with the dimensionless time $\tau \equiv t/\tau_0$ (t is the product of the number of steps and δt). We define $Re_0 \equiv 2\pi v^0_{rms}/\nu$ to be the value of the initial 'box-size' Reynolds number (here Re_0 equals 932965). Our results are obtained for times $t_0 \leq t << t_*$, where t_* is the time at which the (growing) integral scale $L(t) \equiv \langle (\sum_{\mathbf{k}} |\mathbf{v}(\mathbf{k}, t)|^2/k) / \sum_{\mathbf{k}} |\mathbf{v}(\mathbf{k}, t)|^2 \rangle$ becomes of the order of the linear size of the simulation box. For times $t \gtrsim t_*$, finite-size effects which might well be non-universal, modify the numerical results, and are not considered here.

---

*Electronic address: kalelkar@physics.iisc.ernet.in

In Fig. 1, we show some preliminary results that serve as a check of our numerical method and parameter values (which were chosen to ensure linear stability of the numerical scheme). Figure 1(a) shows on a log-log plot, the scaled kinetic energy spectrum $k^{5/3}E(k,\tau)$ as a function of the wavenumber k. On starting with the spectrum specified above, a cascade of energy is seen to large wavenumbers. The plots are equispaced in time with a temporal separation of $\tau = 0.24$. The plot with open circles is calculated at cascade completion at dimensionless time $\tau = \tau_c = 0.71$, and shows a wavenumber range (for $1 \lesssim k \lesssim 10$) that exhibits the well-known $-5/3$ power-law[8]. Upon cascade completion, the shape of the energy spectrum does not change appreciably (except at large wavenumbers where it falls), but the kinetic energy decays. In Fig. 1(b), we plot the normalized kinetic energy $E(\tau)/E_0$ as a function of the dimensionless time τ, which is found to decay monotonically[8]. In Fig. 1(c), we plot the normalized kinetic energy-dissipation rate $\epsilon(\tau)/\epsilon_0$ [$\epsilon(t) \equiv \sum_{\mathbf{k}} k^2 |\mathbf{v}(\mathbf{k}, t)|^2$] as a function of the dimensionless time τ. The kinetic energy-dissipation rate peaks[8, 9] at $\tau = \tau_c$, corresponding to cascade completion in the energy spectrum, and decreases thereafter. The turbulence may be considered as 'fully developed' at $\tau = \tau_c$ and our spatial results (see below) will be calculated at this instant of time.

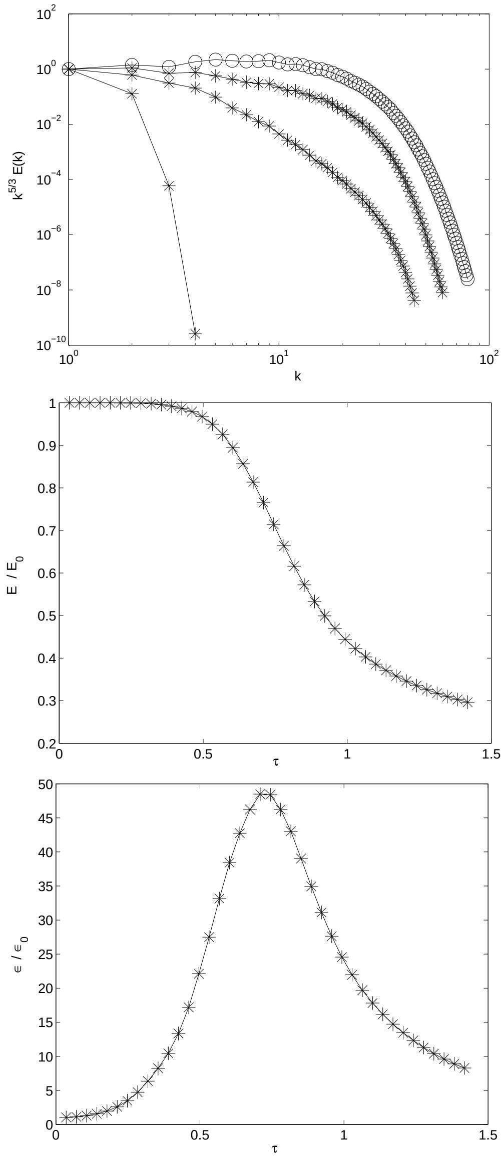

FIG. 1: (a) Log-log plot of the temporal evolution of the scaled kinetic energy spectrum $k^{5/3}E(k,\tau)$ as a function of the wavenumber k at temporal separations of $\tau = 0.24$, with $E(k, t_0) \sim k^4 e^{-2k^2}$. The plot with open circles is calculated at cascade completion, at dimensionless time $\tau = \tau_c = 0.71$. (b) Plot of the normalized kinetic energy $E(\tau)/E_0$ as a function of the dimensionless time τ, with $E(k, t_0) \sim k^4 e^{-2k^2}$. (c) Plot of the normalized kinetic energy-dissipation rate $\epsilon(\tau)/\epsilon_0$ as a function of the dimensionless time τ, with $E(k, t_0) \sim k^4 e^{-2k^2}$.

B. Vorticity

The dynamics of vortex structures in a turbulent flow-field is governed by the response of the vorticity vector to the strain-rate tensor. In Fig. 2(a), we plot the normalized probability distribution $P(|\omega|)$ of $|\omega|$ at cascade completion. The distribution is found to peak at $|\omega| = 1.5\sigma$

(σ denotes the standard deviation) and has an exponential tail for $|\omega| > 1.5\sigma$ with a fit $P(|\omega|) \sim e^{-\beta|\omega|^{\alpha}}$, $\beta = 0.05 \pm 0.01$, $\alpha = 1.00 \pm 0.01$ (error-bars from a least-squares fit). In Fig. 2(b), we plot iso-$|\omega|$ surfaces for the isovalue $|\omega| = \langle|\omega|\rangle$ (angular brackets denote a volume average) at cascade completion, which appear to be crumpled sheet-like structures (found throughout the isovalue range $[\langle|\omega|\rangle - \sigma, \langle|\omega|\rangle + \sigma]$). At early times $\tau << \tau_c$, regions of intense vorticity (with the isovalue $|\omega| = \langle|\omega|\rangle + 2\sigma$) were found to be sheet-like (see Fig. 3(a)). It is plausible that a small volume fraction[14] of such structures, subject to shear and stretching, 'roll-up' to form the filaments visualised in Fig. 3(b) at cascade completion. The filaments are found to be of diameter of the order of the grid spacing, and have a contour length that occasionally extends nearly to the linear size of the simulation box[15]. We choose to quote dimensions of the structures relative to the (fixed) box-size and the grid-spacing, since both the dissipative and the integral length scales vary in time, in decaying turbulence. Iso-$|\omega|$ surfaces in the range $|\omega| < (\langle|\omega|\rangle - \sigma)$ were not found to exhibit any particular structure at cascade completion. The above results are in accordance with earlier studies of statistically steady[1, 2, 3, 4] and decaying[8, 9] turbulence.

C. Strain-Rate Tensor

At each grid point, we compute the eigenvalues λ_1, λ_2 and λ_3 (with the convention $\lambda_1 \geq \lambda_2 \geq \lambda_3$) of the strain-rate tensor S_{ij}, and the corresponding orthonormal eigenvectors e_1, e_2, and e_3. In a constant-density flow, incompressibility requires that $\sum_i \lambda_i = 0$, with $\lambda_1 > 0$, $\lambda_3 < 0$, the sign of the intermediate eigenvalue λ_2 being indeterminate. In Fig. 4(a), we plot the normalized probability distribution $P(\lambda_i)$ of the eigenvalues λ_i at cascade completion. We find that λ_2 has a positive mean. The statistically preferred ratio of the mean strain-rates $\langle\lambda_1\rangle : \langle\lambda_2\rangle : \langle\lambda_3\rangle$ was found to equal $4.9 : 1 : -5.9$ at cascade completion[16].

In Fig. 4(b), we plot the normalized probability distribution $P[\cos(\omega, e_i)]$ of cosine of the angle between ω and the eigenvectors e_i, at cascade completion. We observe that ω is preferentially aligned (or antialigned) with eigenvector e_2 (a peak-to-valley ratio ≈ 5.1 was found) corresponding to eigenvalue λ_2 of *minimum* relative mean strain-rate (disregarding the sign in the mean ratio, which merely indicates an extensional or compressional strain on the fluid element). The vorticity is also found to be preferentially perpendicular to eigenvector e_3 corresponding to the principal compressive eigenvalue λ_3, while no specific angular relationship is observed relative to eigenvector e_1. We could confirm an earlier result[3] that the preferential alignment of ω with e_2 is already pronounced *during* the cascade process, much prior to the appearance of distinct filaments in regions of intense vorticity. In Fig. 4(c), we plot $P[\cos(\omega, e_i)]$ at cascade completion, for a run with the same parameter values as in Section II(A), but without hyperviscosity (here $\nu = 10^{-4}$). We find that the inclusion of hyperviscosity introduces no qualitative changes (a peak-to-valley ratio of 5.3 was found), and we believe that effects on structural properties are minimal. The positive mean of λ_2, the ratio of the mean strain-rates, and the preferential alignment of ω with e_2 is consistent with corresponding observations in statistically steady[3] and decaying[7] turbulence.

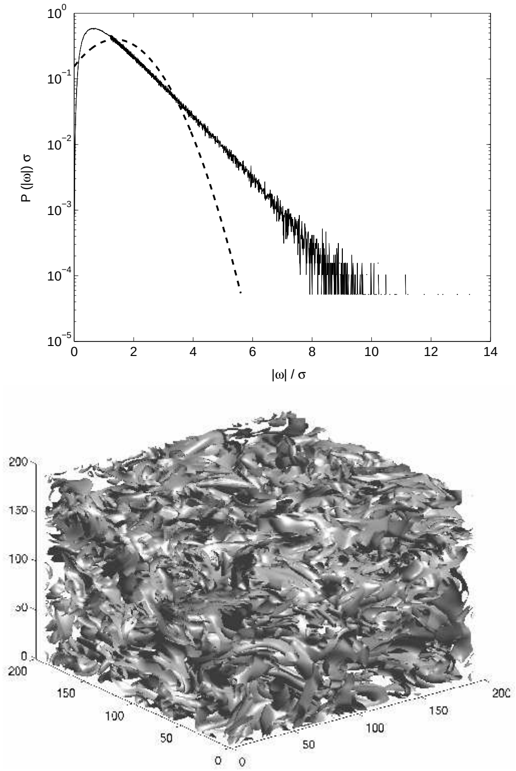

FIG. 2: (a) Semilog plot of the normalized probability distribution $P(|\omega|)$ of $|\omega|$ (ω is the vorticity) at cascade completion, with $E(k, t_0) \sim k^4 e^{-2k^2}$. The dashed-line plot is a normalized Gaussian distribution for comparison.
(b) Plot of iso-$|\omega|$ surfaces for the isovalue $|\omega| = \langle|\omega|\rangle$ at cascade completion, with $E(k, t_0) \sim k^4 e^{-2k^2}$.

D. Mean Enstrophy Production Rate

In a classical work[17], Betchov derived an equation for the rate of production of the mean enstrophy $\langle\omega^2\rangle$[18] in unforced, incompressible, homogeneous, and isotropic turbulence, viz.

$$\frac{\partial\langle\omega^2\rangle}{\partial t} = -\langle\lambda_1\lambda_2\lambda_3\rangle - \frac{\nu}{4}\left\langle\left(\frac{\partial^2 v_i}{\partial x_j \partial x_k}\right)^2\right\rangle, \quad (2)$$

where the angular brackets denote a volume average. From Eq. (2), it is evident that production of $\langle\omega^2\rangle$ requires a predominantly negative value of $\lambda_1\lambda_2\lambda_3$ in the

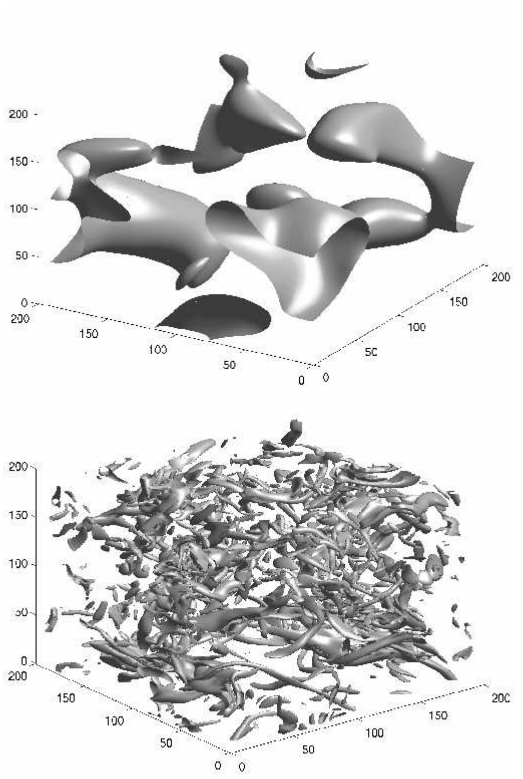

FIG. 3: (a) Plot of iso-$|\omega|$ surfaces for the isovalue $|\omega| = \langle|\omega|\rangle + 2\sigma$ (σ is the standard deviation) at dimensionless time $\tau << \tau_c$, with $E(k, t_0) \sim k^4 e^{-2k^2}$.
(b) Plot of iso-$|\omega|$ surfaces for the isovalue $|\omega| = \langle|\omega|\rangle + 2\sigma$ at cascade completion, with $E(k, t_0) \sim k^4 e^{-2k^2}$.

fluid. In Fig. 5(a), we plot the normalized probability distribution $P(\lambda_1\lambda_2\lambda_3)$ of $\lambda_1\lambda_2\lambda_3$ at cascade completion and find that the distribution has a negative mean (with a skewness equal to -7.83), a result that has already been noted in an early numerical study[19]. If $\lambda_1\lambda_2\lambda_3$ is positive, we have one positive and two negative eigenvalues: a vortex element is stretched along one direction and squashed along the other two, forming a slender filamentary structure. If $\lambda_1\lambda_2\lambda_3$ is negative, we have one negative and two positive eigenvalues: a vortex element is stretched along two directions and squashed along the third, forming a sheet-like structure. In homogeneous turbulence $\langle\lambda_1\lambda_2\lambda_3\rangle$ is found to be negative[17, 20], indicating a predominance of sheet-like structures, which accords with Fig. 2(b). In Fig. 5(b), we plot $-\langle\lambda_1\lambda_2\lambda_3\rangle$ as a function of the dimensionless time τ. We find that the magnitude of $-\langle\lambda_1\lambda_2\lambda_3\rangle$ peaks at cascade completion ($\tau = 0.71$), which is consistent with the dimensionless time at which the kinetic energy-dissipation rate is a maximum (cf. Fig. 1(c)). In homogeneous turbulence, the term $-\langle\lambda_1\lambda_2\lambda_3\rangle$ can be shown[17] to equal the expression $\langle\omega_i\omega_j S_{ij}\rangle = \sum_i\langle\lambda_i(\omega\cdot e_i)^2\rangle$. In Fig. 5(c), we plot $\langle\lambda_i(\omega\cdot e_i)^2\rangle$, the rates of production of the mean enstrophy along eigenvectors e_i, and find that the production rate is largest along eigenvector e_2 corresponding to eigenvalue λ_2 of *minimum* relative mean strain-rate (see above), a remarkable result that appears to be new.

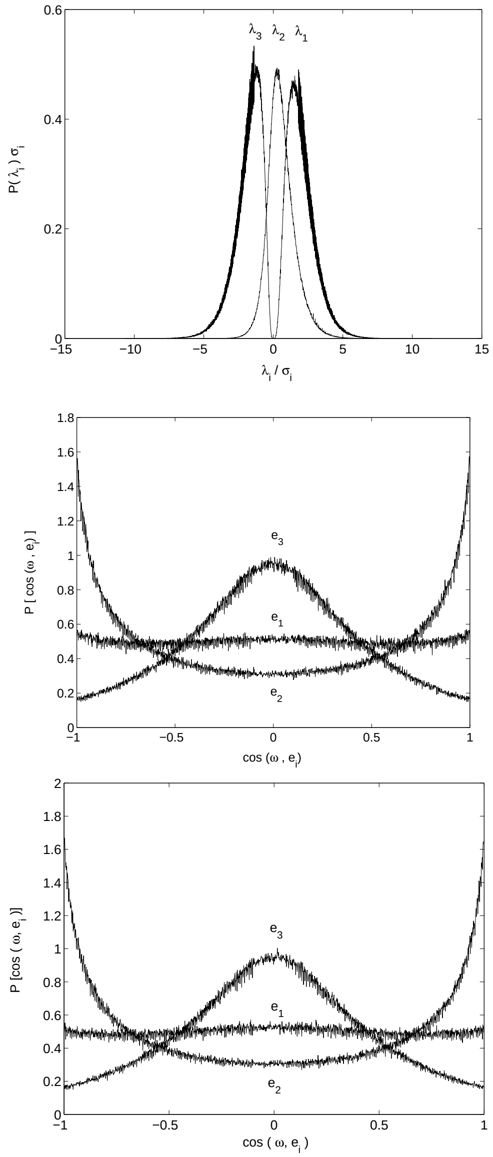

FIG. 4: (a) Plot of the normalized probability distribution $P(\lambda_i)$ of the eigenvalues λ_i of the strain-rate tensor S_{ij}, $i, j = 1, 2, 3$, at cascade completion, with $E(k, t_0) \sim k^4 e^{-2k^2}$.
(b) Plot of the normalized probability distribution of cosine of the angle between ω and the eigenvectors e_i of S_{ij} at cascade completion, with $E(k, t_0) \sim k^4 e^{-2k^2}$.
(c) Plot of the normalized probability distribution of cosine of the angle between ω and the eigenvectors e_i at cascade completion, with $E(k, t_0) \sim k^4 e^{-2k^2}$ and without hyperviscosity.

From Fig. 5(b) we observe that the mean enstrophy production rate $-\langle\lambda_1\lambda_2\lambda_3\rangle$ has an upper bound. In the same work[17], Betchov invoked formal mathematical inequalities and incompressibility to derive the upper bound

$$|\langle\lambda_1\lambda_2\lambda_3\rangle| \le \frac{1}{3\sqrt{6}}\langle(\lambda_1^2 + \lambda_2^2 + \lambda_3^2)^{3/2}\rangle. \qquad (3)$$

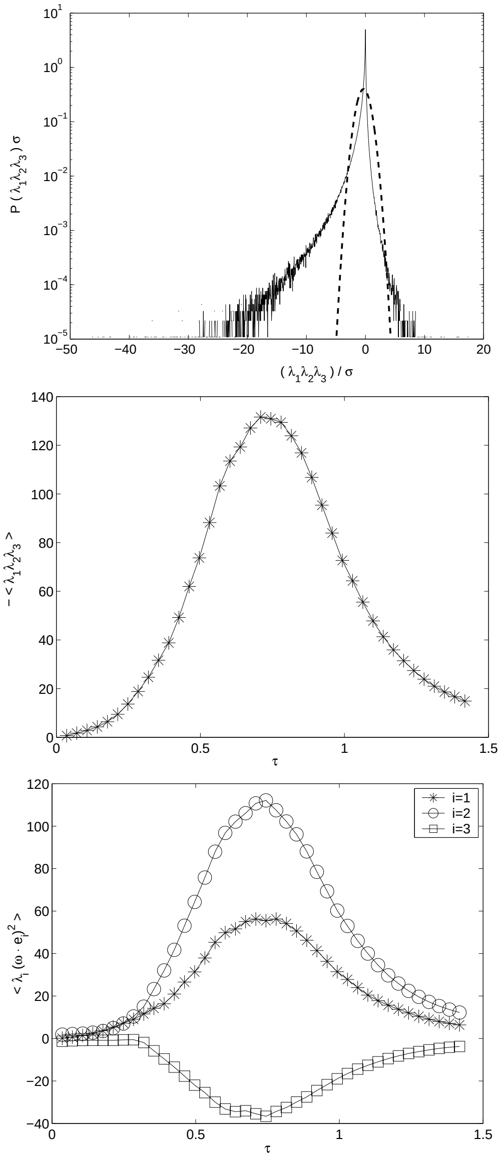

FIG. 5: (a) Semilog plot of the normalized probability distribution $P(\lambda_1\lambda_2\lambda_3)$ of $\lambda_1\lambda_2\lambda_3$ at cascade completion, with $E(k,t_0) \sim k^4e^{-2k^2}$. The dashed-line plot is a normalized Gaussian distribution for comparison.
(b) Plot of $-\langle\lambda_1\lambda_2\lambda_3\rangle$ (see Eq. (2)) as a function of the dimensionless time τ, with $E(k,t_0) \sim k^4e^{-2k^2}$.
(c) Plot of the rates of production of the mean enstrophy $\langle\lambda_i(\omega\cdot e_i)^2\rangle$ along the eigenvectors e_i of S_{ij}, as a function of the dimensionless time τ, with $E(k,t_0) \sim k^4e^{-2k^2}$.

The upper bound is the largest rate of production of mean enstrophy compatible with the requirements of isotropy, homogeneity, and incompressibility. In Fig. 6, we plot inequality (3)[21] as a function of the dimensionless time τ and find that the inequality is satisfied to a greater degree *during* the cascade process, and for dimensionless times $\tau \gtrsim \tau_c$ asymptotes to the value ≈ 0.57. Dynamical effects suggest an inequality that is stronger than the one due to Betchov.

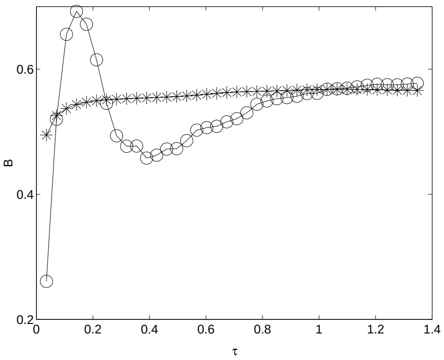

FIG. 6: Plot of Betchov's inequality $B \equiv 3\sqrt{6}|\langle\lambda_1\lambda_2\lambda_3\rangle|/\langle(\lambda_1^2+\lambda_2^2+\lambda_3^2)^{3/2}\rangle \leq 1$ as a function of the dimensionless time τ, with $E(k,t_0) \sim k^4e^{-2k^2}$ (open circles) and $E(k,t_0) \sim k$ (asterisks).

III. POWER-LAW SPECTRUM

A. Numerical Method

We use the numerical scheme, spectral resolution, step size, viscosities, and boundary conditions as specified in Section II(A). The initial velocity field is taken to be $\mathbf{v}(\mathbf{k},t_0) \sim k^{1/2}e^{i\phi_{\mathbf{k}}}$, with $\phi_{\mathbf{k}}$ random variables distributed uniformly between 0 and 2π, which corresponds to the initial energy spectrum $E(k,t_0) \sim k$ (with $E(k,t) \equiv |\mathbf{v}(\mathbf{k},t)|^2$). Here, the dimensionless time τ_0 equals 13.9 and the initial 'box-size' Reynolds number Re_0 equals 350181. Our results are obtained for times $t_0 \leq t << t_*$, and we choose to calculate our spatial results at dimensionless time $\tau = \tau_c = 0.71$[22] which is equal to the dimensionless time at which the kinetic energy-dissipation rate peaks, on starting with a 'cascade-type' spectrum as shown in Fig. 1(c).

In Fig. 7(a), we show on a log-log plot, the kinetic energy spectrum $E(k,\tau)$ as a function of the wavenumber k. The plots are equispaced in time with a temporal separation of $\tau = 0.24$ and the plot with open circles is calculated at $\tau = \tau_c$. The spectrum does not cascade to large wavenumbers or exhibit a wavenumber range with a $-5/3$ power-law at any stage of temporal evolution. In Figs. 7(b) and (c), we plot the normalized kinetic energy $E(\tau)/E_0$ and the normalized kinetic energy-dissipation rate $\epsilon(\tau)/\epsilon_0$, as a function of the dimensionless time τ (plotted on a linear scale in order to compare with Figs. 1(b) and (c)). The kinetic energy $E(\tau)$ is found to decay as a power-law (on a log-log plot) with an exponent equal to -0.91 ± 0.04, with error-bars from a least-squares fit. The exponent is theoretically predicted[11] to equal -1, and we believe the discrepancy is due to the low spectral resolution of our DNS. The normalized kinetic energy-

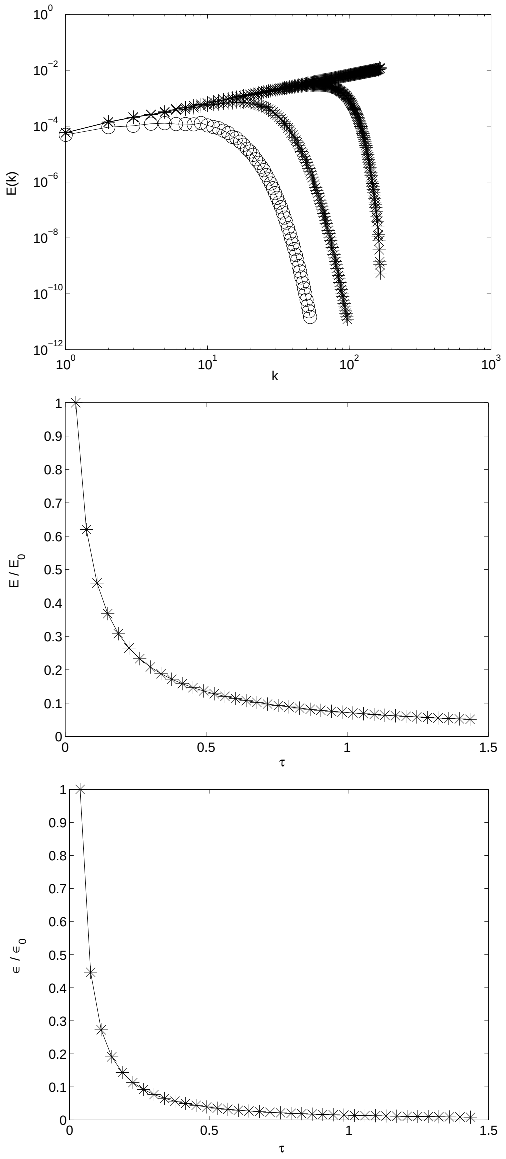

FIG. 7: (a) Log-log plot of the temporal evolution of the kinetic energy spectrum $E(k,\tau)$ as a function of the wavenumber k at temporal seperations of $\tau = 0.24$, with $E(k,t_0) \sim k$. The plot with open circles is calculated at dimensionless time $\tau = \tau_c = 0.71$.
(b) Plot of the temporal evolution of the normalized kinetic energy $E(\tau)/E_0$ as a function of the dimensionless time τ, with $E(k,t_0) \sim k$.
(c) Plot of the normalized kinetic energy-dissipation rate $\epsilon(\tau)/\epsilon_0$ as a function of the dimensionless time τ, with $E(k,t_0) \sim k$.

dissipation rate $\epsilon(\tau)/\epsilon_0$ does not exhibit a peak (cf. Fig. 1(c)) and decays monotonically.

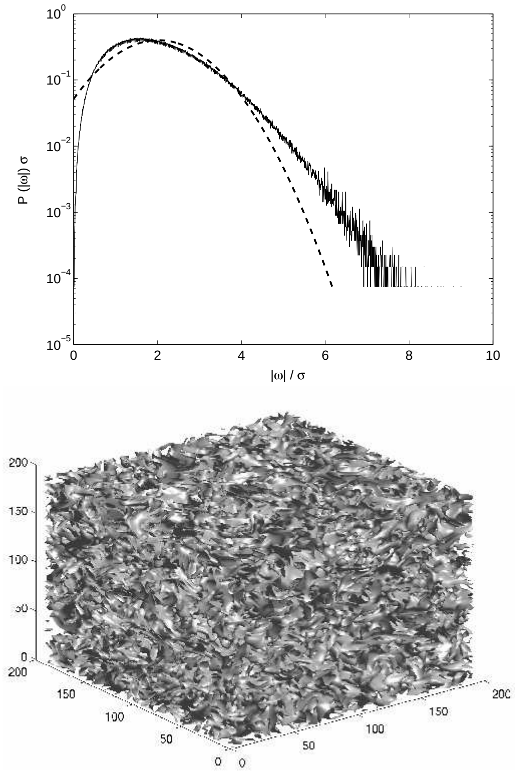

FIG. 8: (a) Semilog plot of the normalized probability distribution $P(|\omega|)$ of $|\omega|$ (ω is the vorticity) at dimensionless time $\tau = \tau_c$, with $E(k,t_0) \sim k$. The dashed-line plot is a normalized Gaussian distribution for comparison.
(b) Plot of iso-$|\omega|$ surfaces for the isovalue $|\omega| = \langle|\omega|\rangle$ at $\tau = \tau_c$, with $E(k,t_0) \sim k$.

B. Vorticity

In Fig. 8(a), we plot the normalized probability distribution $P(|\omega|)$ of $|\omega|$ (ω is the vorticity) at $\tau = \tau_c$. The distribution peaks at $|\omega| = 1.5\sigma$ as in Fig. 2(a), however it does not exhibit a stretched-exponential tail. In Fig. 8(b), we plot iso-$|\omega|$ surfaces for the isovalue $|\omega| = \langle|\omega|\rangle$ at $\tau = \tau_c$, which appear to be shredded sheet-like structures (observed throughout the isovalue range $[\langle|\omega|\rangle - \sigma, \langle|\omega|\rangle + \sigma]$). At early times $\tau << \tau_c$, regions of intense vorticity (with the isovalue $|\omega| = \langle|\omega|\rangle + 2\sigma$) were found to be structure-less 'blobs' of length of the order of the grid spacing (see Fig. 9(a)), in contrast to the sheet-like structures in Fig. 3(a). At $\tau = \tau_c$, isosurfaces of intense vorticity (in Fig. 9(b)), appear to be roughly ellipsoidal in shape with semiaxes of the order of the grid spacing and differ markedly from the coherent filaments in the 'cascade-type' case shown in Fig. 3(b).

C. Strain-Rate Tensor

In Fig. 10(a), we plot the normalized probability distribution $P(\lambda_i)$ of the eigenvalues λ_i of the strain-rate

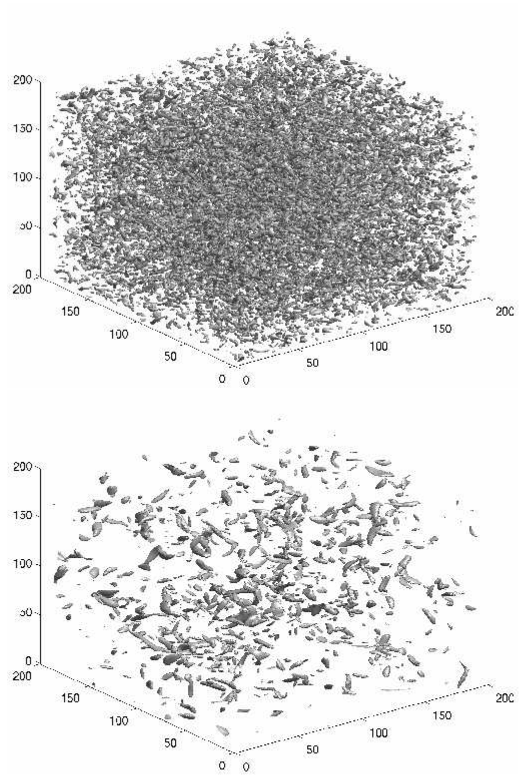

FIG. 9: (a) Plot of iso-$|\omega|$ surfaces for the isovalue $|\omega| = \langle|\omega|\rangle + 2\sigma$ (σ is the standard deviation), at dimensionless time $\tau << \tau_c$, with $E(k,t_0) \sim k$.
(b) Plot of iso-$|\omega|$ surfaces for the isovalue $|\omega| = \langle|\omega|\rangle + 2\sigma$ at $\tau = \tau_c$, with $E(k,t_0) \sim k$.

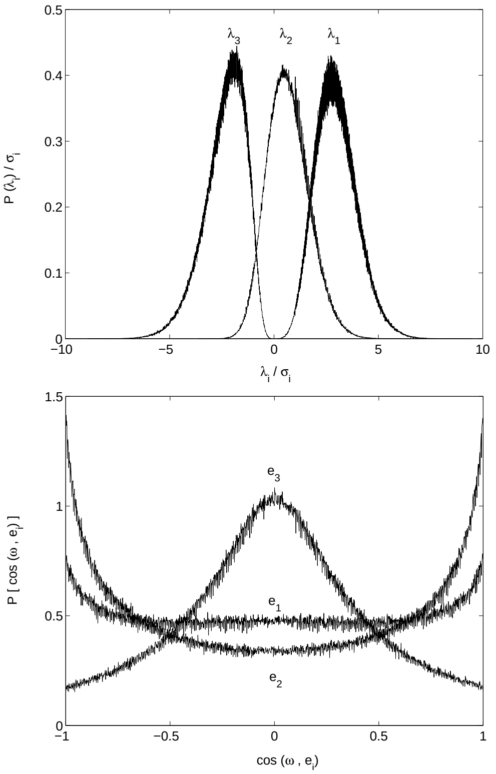

FIG. 10: (a) Plot of the normalized probability distribution $P(\lambda_i)$ of the eigenvalues λ_i of the strain-rate tensor S_{ij}, $i,j = 1,2,3$, at dimensionless time $\tau = \tau_c$, with $E(k,t_0) \sim k$.
(b) Plot of the normalized probability distribution of cosine of the angle between ω and the eigenvectors e_i of S_{ij} at $\tau = \tau_c$, with $E(k,t_0) \sim k$.

tensor S_{ij} at $\tau = \tau_c$. We find that λ_2 has a positive mean. The statistically preferred ratio of the mean eigenvalues $\langle\lambda_1\rangle : \langle\lambda_2\rangle : \langle\lambda_3\rangle$ was found to equal $4.6 : 1 : -5.6$, which differs only marginally from that obtained in the 'cascade-type' case. In Fig. 10(b), we plot the normalized probability distribution of cosine of the angle between ω and the eigenvectors e_i of S_{ij} at $\tau = \tau_c$. As in Fig. 4(b), we observe that ω is preferentially parallel (or antiparallel) to e_2 (with a reduced peak-to-valley ratio ≈ 4.1) and perpendicular to e_3, while no specific angular relationship is observed relative to e_1 (though we note a small probability of alignment at $\cos(\omega, e_1) = \pm 1$).

D. Mean Enstrophy Production Rate

In Fig. 11(a), we plot the normalized probability distribution $P(\lambda_1\lambda_2\lambda_3)$ of $\lambda_1\lambda_2\lambda_3$ at $\tau = \tau_c$. As in Fig. 5(a), we find that the distribution has a negative mean (a relatively smaller skewness equal to -3.90 was found). In Fig. 11(b), we plot the value of $-\langle\lambda_1\lambda_2\lambda_3\rangle$ (see Eq. (2)) as a function of the dimensionless time τ and find that it decreases monotonically, in contrast to Fig. 5(b). In Fig. 11(c), we plot $\langle\lambda_i(\omega\cdot e_i)^2\rangle$, the rates of production of the mean enstrophy along eigenvectors e_i as a function of the dimensionless time τ, and find that the production rates *decrease* monotonically along all the principal axis directions, in remarkable contrast to Fig. 5(c). In Fig. 6, we plot inequality (3) as a function of the dimensionless time τ, and find that the inequality monotonically approaches the same asymptotic value ≈ 0.57 as in the 'cascade-type' case.

E. Crossover

From Figs. 1(c) and 7(c), it is evident that some representative set of initial energy spectra may be utilised to exhibit a crossover from non-'cascade-type' to 'cascade-type' behaviour, with the kinetic energy-dissipation rate serving as a diagnostic. In particular, one may choose the set $E(k,t_0) \sim k^q e^{-k^q}$ with parameter q. In Fig. 12, we plot $\epsilon(\tau)/\epsilon_0$ as a function of the dimensionless time τ (with τ_0 calculated using the initial energy spectrum with $q = 0.4$). On varying q in the range $[0.4, 0.8]$, we find that $\epsilon(\tau)/\epsilon_0$ exhibits a smooth crossover at $q \approx 0.6$ from non-'cascade-type' to 'cascade-type' behaviour.

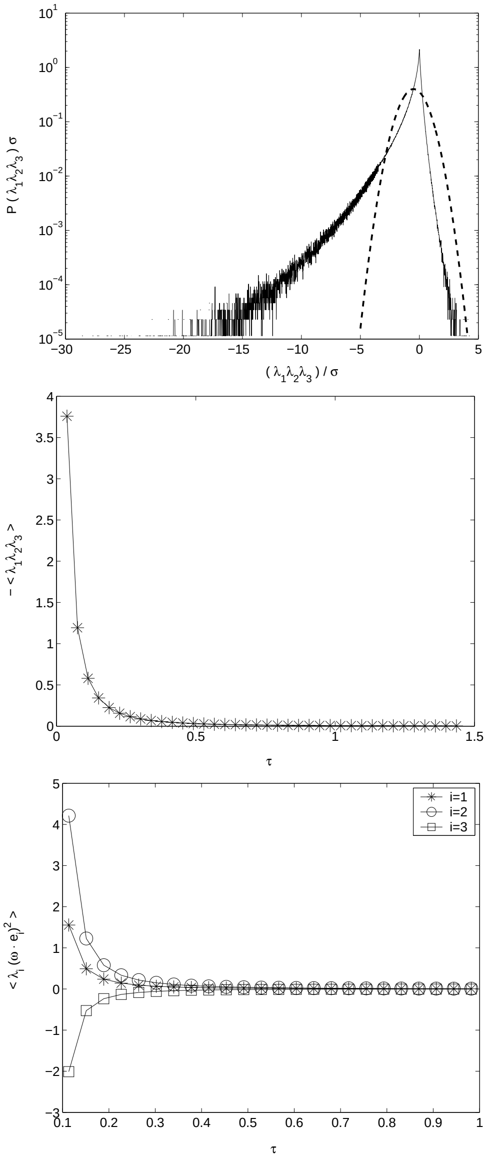

FIG. 11: (a) Semilog plot of the normalized probability distribution $P(\lambda_1\lambda_2\lambda_3)$ of $\lambda_1\lambda_2\lambda_3$, with $E(k,t_0) \sim k$. The dashed-line plot is a normalized Gaussian distribution for comparison.
(b) Plot of $-\langle\lambda_1\lambda_2\lambda_3\rangle$ (see Eq. (2)) as a function of the dimensionless time τ, with $E(k,t_0) \sim k$.
(c) Plot of the rates of production of the mean enstrophy $\langle\lambda_i(\omega \cdot e_i)^2\rangle$ along the eigenvectors e_i of S_{ij}, as a function of the dimensionless time τ, with $E(k,t_0) \sim k$.

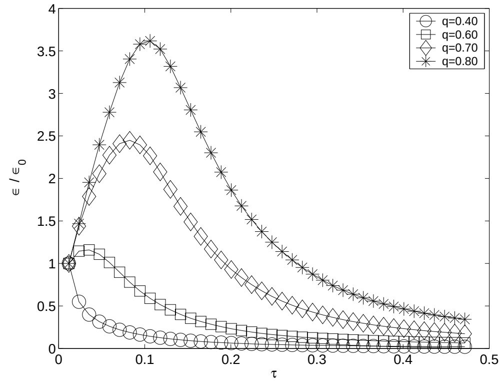

FIG. 12: Plot of the normalized kinetic energy-dissipation rate $\epsilon(\tau)/\epsilon_0$ as a function of the dimensionless time τ, with $E(k,t_0) \sim k^q e^{-k^q}$, $0.4 \leq q \leq 0.8$.

IV. CONCLUSIONS

To summarize, we have presented results from a systematic numerical study of structural properties of an unforced, incompressible, homogeneous, and isotropic turbulent fluid with an initial energy spectrum that develops a cascade to large wavenumbers. The results are contrasted with those from the power-law initial spectra investigated in Refs. [10, 11], which do not exhibit such a cascade. Differences are noted in plots of vorticity isosurfaces, the temporal evolution of the kinetic energy-dissipation rate, and the rates of production of the mean enstrophy along the principal axes of the strain-rate tensor. However, preferential alignment of the vorticity vector with the intermediate eigenvector of the strain-rate tensor is found to be unchanged. A crossover between non-‘cascade-type’ and ‘cascade-type’ behaviour is shown numerically for a specific set of initial energy spectra. Our study shows that decaying turbulence is strikingly different for different types of initial conditions. Initial conditions that lead to a cascade yield features similar to those obtained in the statistically steady case. However, power-law initial conditions that do not lead to an energy cascade exhibit several qualitatively new features which we have described above.

Acknowledgments

The author thanks T. Kalelkar, R. Pandit, and R. Govindarajan for discussions, D. Mitra for the code, SERC (IISc) for computational resources, and CSIR (India) for financial support.

---

[1] S. Douady, Y. Couder, and M. Brachet, Phys. Rev. Lett., **67**, 983 (1991); E. Villermaux, B. Sixou, and Y. Gagne, Phys. Fluids, **7**, 2008 (1995).

[2] E. Siggia, J. Fluid Mech., **107**, 375 (1981); Z. She, E. Jackson, and S. Orszag, Nature, **344**, 226 (1990).

[3] A. Vincent and M. Meneguzzi, J. Fluid Mech., **225**, 1 (1991).

[4] J. Jimenez, A. Wray, P. Saffman, and R. Rogallo, J. Fluid Mech., **255**, 65 (1993).

[5] A. Kolmogorov, Dokl. Akad. Nauk. SSSR, **32**, 1 (1941) [Proc. R. Soc. London, Ser. A, **434**, 15 (1991)].

[6] A. Monin and A. Yaglom, *Statistical Fluid Mechanics*, edited by J. Lumley, (MIT Press, Cambridge, 1975), Vol. 2.

[7] W. Ashurst, A. Kerstein, R. Kerr, and C. Gibson, Phys. Fluids, **30**, 2343 (1987); A. Tsinober, E. Kit, and T. Dracos, J. Fluid Mech., **242**, 169 (1992).

[8] K. Yamamoto and I. Hosokawa, J. Phys. Soc. Jpn., **57**, 1532 (1988).

[9] I. Hosokawa, S. Oide, and K. Yamamoto, J. Phys. Soc. Jpn., **66**, 2961 (1997).

[10] C. Kalelkar and R. Pandit, Phys. Rev. E, **69**, 046304 (2004).

[11] P. Ditlevsen, M. Jensen, and P. Olesen, Physica A, **342**, 471 (2004).

[12] P. Olesen, Phys. Lett. B, **398**, 321 (1997).

[13] S. Dhar, A. Sain, and R. Pandit, Phys. Rev. Lett., **78**, 2964 (1997).

[14] In Ref. [4] it has been shown that filamentary structures in regions of intense vorticity contain only a small percentage of the total enstrophy.

[15] In Ref. [9], filamentary structures are visualized in a 512^3 DNS of decaying turbulence.

[16] We note that in Refs. [7], the strain-rate eigenvalue ratio was found to equal $3:1:-4$ based on the most probable values, as opposed to the mean.

[17] R. Betchov, J. Fluid Mech., **1**, 497 (1956).

[18] The analogous equation for the mean-squared strain-rate $\langle s^2\rangle \equiv \langle S_{ij}S_{ij}\rangle$ is redundant since $\langle s^2\rangle = \langle \omega^2\rangle/2$ in homogeneous, incompressible flows. The probability distribution $P(|s|)$, $|s| \equiv \sqrt{S_{ij}S_{ij}}$ was found to resemble $P(|\omega|)$.

[19] R. Betchov, Phys. Fluids, **18**, 1230 (1975).

[20] A. Townsend, Proc. R. Soc. London, Ser. A, **208**, 534 (1951).

[21] Betchov in fact states that the inequality (3) "cannot be measured by conventional methods" (p. 499, Ref. [17]) and introduces a *weaker* inequality which he tests through hot-wire anemometry. Clearly, there is no difficulty in directly testing inequality (3) in a DNS.

[22] At dimensionless time $\tau = \tau_c$, the Reynolds number Re were found to be of the same order of magnitude in both 'cascade-type' and 'power-law' cases.